

MIT Open Access Articles

Aag DNA Glycosylase Promotes Alkylation-Induced Tissue Damage Mediated by Parp1

The MIT Faculty has made this article openly available. **Please share** how this access benefits you. Your story matters.

Citation: Calvo, Jennifer A., Catherine A. Moroski-Erkul, Annabelle Lake, Lindsey W. Eichinger, Dharini Shah, Iny Jhun, Prajit Limsirichai, et al. Aag DNA Glycosylase Promotes Alkylation-Induced Tissue Damage Mediated by Parp1. Edited by Samuel H. Wilson. PLoS Genetics 9, no. 4 (April 4, 2013): e1003413.

As Published: <http://dx.doi.org/10.1371/journal.pgen.1003413>

Publisher: Public Library of Science

Persistent URL: <http://hdl.handle.net/1721.1/79393>

Version: Author's final manuscript: final author's manuscript post peer review, without publisher's formatting or copy editing

Terms of use: Creative Commons Attribution



Aag DNA Glycosylase Promotes Alkylation-Induced Tissue Damage Mediated by Parp1

Jennifer A. Calvo^{1,2}, Catherine A. Moroski-Erkul^{1,2}, Annabelle Lake^{1,2,3}, Lindsey W. Eichinger^{1,2}, Dharini Shah^{1,2}, Iny Jhun^{1,2}, Prajit Limsirichai^{1,2}, Roderick T. Bronson⁴, David C. Christiani⁵, Lisiane B. Meira^{1,2,3}, Leona D. Samson^{1,2,6,7*}

1 Department of Biological Engineering, Massachusetts Institute of Technology, Cambridge, Massachusetts, United States of America, **2** Center for Environmental Health Sciences, Massachusetts Institute of Technology, Cambridge, Massachusetts, United States of America, **3** Faculty of Health and Medical Sciences, University of Surrey, Guildford, United Kingdom, **4** Department of Pathology, Harvard Medical School, Cambridge, Massachusetts, United States of America, **5** Department of Environmental Health, Harvard School of Public Health, Boston, Massachusetts, United States of America, **6** Department of Biology, Massachusetts Institute of Technology, Cambridge, Massachusetts, United States of America, **7** The David H. Koch Institute for Integrative Cancer Research, Massachusetts Institute of Technology, Cambridge, Massachusetts, United States of America

Abstract

Alkylating agents comprise a major class of front-line cancer chemotherapeutic compounds, and while these agents effectively kill tumor cells, they also damage healthy tissues. Although base excision repair (BER) is essential in repairing DNA alkylation damage, under certain conditions, initiation of BER can be detrimental. Here we illustrate that the alkyladenine DNA glycosylase (AAG) mediates alkylation-induced tissue damage and whole-animal lethality following exposure to alkylating agents. Aag-dependent tissue damage, as observed in cerebellar granule cells, splenocytes, thymocytes, bone marrow cells, pancreatic β -cells, and retinal photoreceptor cells, was detected in wild-type mice, exacerbated in *Aag* transgenic mice, and completely suppressed in *Aag*^{-/-} mice. Additional genetic experiments dissected the effects of modulating both BER and Parp1 on alkylation sensitivity in mice and determined that Aag acts upstream of Parp1 in alkylation-induced tissue damage; in fact, cytotoxicity in WT and *Aag* transgenic mice was abrogated in the absence of Parp1. These results provide *in vivo* evidence that Aag-initiated BER may play a critical role in determining the side-effects of alkylating agent chemotherapies and that Parp1 plays a crucial role in Aag-mediated tissue damage.

Citation: Calvo JA, Moroski-Erkul CA, Lake A, Eichinger LW, Shah D, et al. (2013) Aag DNA Glycosylase Promotes Alkylation-Induced Tissue Damage Mediated by Parp1. *PLoS Genet* 9(4): e1003413. doi:10.1371/journal.pgen.1003413

Editor: Samuel H. Wilson, National Institute of Environmental Health Sciences, United States of America

Received: January 2, 2013; **Accepted:** February 11, 2013; **Published:** April 4, 2013

Copyright: © 2013 Calvo et al. This is an open-access article distributed under the terms of the Creative Commons Attribution License, which permits unrestricted use, distribution, and reproduction in any medium, provided the original author and source are credited.

Funding: This work was supported by NIH grants R01-CA075576, R01-CA055042, R01-CA149261, P30-ES00002, and P30-ES02109 (to LDS). The human blood sample portion was conducted at the Harvard Catalyst Clinical Research Center at Massachusetts Institute of Technology and was supported by grant numbers M01RR-01066 and UL1 RR025758—Harvard Clinical and Translational Science Center, from the National Center for Research Resources. The content is solely the responsibility of the authors and does not necessarily represent the official views of the National Center for Research Resources or the National Institutes of Health. Experiments performed at the University of Surrey were provided by a grant from the Royal Society to LBM. LDS is an American Cancer Society Research Professor. The funders had no role in study design, data collection and analysis, decision to publish, or preparation of the manuscript.

Competing Interests: The authors have declared that no conflict of interest exists.

* E-mail: lsamson@mit.edu

Introduction

DNA damage continually arises from environmental agents and reactive byproducts of normal cellular function. Moreover, DNA damage is deliberately induced during the course of cancer chemotherapy. Such damage can result in cell death, mutagenesis, and genetic instability thus promoting tissue degeneration, aging, cancer, and sometimes death. DNA repair pathways have evolved to cope with recurring DNA damage, providing protection against carcinogenesis, neurodegeneration, and premature aging [1–5]. Understandably, loss of function mutations have been extensively studied, whereas genetic variants that result in increased DNA repair activity have not received the same attention, primarily because decreased DNA repair is thought to be more relevant for increased cancer risk. While this concept is accurate for many DNA repair proteins [1–3], a growing body of evidence suggests that increased levels of certain DNA repair enzymes can result in loss of coordination between the enzymatic steps within a

particular DNA repair pathway; such loss of coordination can negatively impact cellular homeostasis [6–9].

The base excision repair (BER) pathway acts on a wide range of DNA base lesions including alkylated, oxidized, and deaminated bases, as well as abasic (AP) sites and DNA single-strand breaks (SSBs) (reviewed in [6,10]). In its most simplified form, BER is coordinated into 4 main steps (Figure 1A). DNA glycosylases recognize and excise specific base lesions by cleaving the N-glycosyl bond, forming an AP site. AP endonuclease (APE1) then hydrolyzes the phosphodiester backbone, generating a single-stranded DNA break (SSB) with 3'OH and 5'deoxyribose-5-phosphate (5'dRP) termini. DNA polymerase β (Pol β) contains a lyase domain that removes the 5'dRP terminus and a polymerase domain that replaces the missing nucleotide. Finally, BER is completed upon ligation of the nick by DNA Ligase I or the Xrcc1/Ligase III α complex (Figure 1A).

Importantly, numerous BER intermediates (AP sites, 5'dRP termini, and SSBs) are toxic if allowed to accumulate rather than

Author Summary

Alkylating agents are genotoxic chemicals that induce both toxic and mutagenic DNA damage through addition of an alkyl group to DNA. Alkylating agents are routinely and successfully used as chemotherapeutic therapies for cancer patients, with one major disadvantage being the significant toxicity induced in non-tumor tissues. Accordingly, identifying factors that modify susceptibility to alkylation-induced toxicity will provide valuable information in designing cancer therapeutic regimens. This study used mouse genetic experiments to investigate whether proteins important in the base excision repair pathway modulate susceptibility to alkylating agents. In addition to whole-animal toxicity at high doses, treatment of mice with alkylating agents resulted in severe damage to numerous tissues including the cerebellum, retina, bone marrow, spleen, thymus, and the pancreas. We illustrate that the DNA glycosylase Aag can actually confer, rather than prevent, alkylation sensitivity at both the whole-animal and tissue level; i.e., *Aag* transgenic animals are more susceptible than wild type, whereas *Aag*-deficient animals are less susceptible than wild type to alkylation-induced toxicity. Further genetic experiments show that the *Aag*-mediated alkylation sensitivity is dependent on Parp1. Given that we observe a wide range of human AAG expression among healthy individuals, this and other base excision repair proteins may be important factors modulating alkylation susceptibility.

being efficiently shuttled through the downstream BER steps (Figure 1A). Both SSBs and AP sites exert their toxicity as a function of blocking transcription and replication [11]. Further, large numbers of SSBs can indirectly induce toxicity through the hyperactivation of poly(ADP-ribose) polymerase 1 (Parp1) [12] (Figure 1B). AP sites can also be mutagenic; although translesion DNA polymerases can prevent toxicity by bypassing AP sites, such bypass can generate point mutations [13–17]. The 5'dRP intermediate is particularly toxic in mouse embryonic fibroblasts (MEFs) and the alkylation sensitivity of *Polβ* deficient MEFs is almost completely suppressed upon expression of the *Polβ* 5'dRP lyase domain [18]. The toxic nature of BER intermediates underscores why this pathway must be tightly regulated and why alterations in any step of the pathway, without compensatory changes in upstream/downstream steps, can result in the accumulation of toxic intermediates. A clear example of this was illustrated by the fact that hypersensitivity to the alkylating agent methyl methanesulfonate (MMS) in *Polβ*^{-/-} MEFs is completely suppressed if BER is not initiated by the alkyladenine DNA glycosylase (AAG, also known as MPG, ANPG) [19]. Therefore, although BER is essential for the repair of many different types of DNA damage, it must be carefully regulated to avoid the accumulation of toxic BER intermediates.

Aag has a wide substrate specificity, excising numerous structurally-diverse lesions, some of which are innocuous (e.g. 7-methylguanine), while others can be replication-blocking and cytotoxic (e.g. 3-methyladenine) [20–27]. The absence of Aag should therefore result in unrepaired alkylated DNA bases that are replication-blocking lesions, thus increasing cytotoxicity; strikingly, the converse is seen in certain *Aag* deficient tissues. *Aag*^{-/-} bone marrow cells are MMS resistant in *ex vivo* survival assays [28], and *Aag*^{-/-} retinal photoreceptor cells are remarkably refractory to MMS-induced death [29]. Thus, when BER is not initiated,

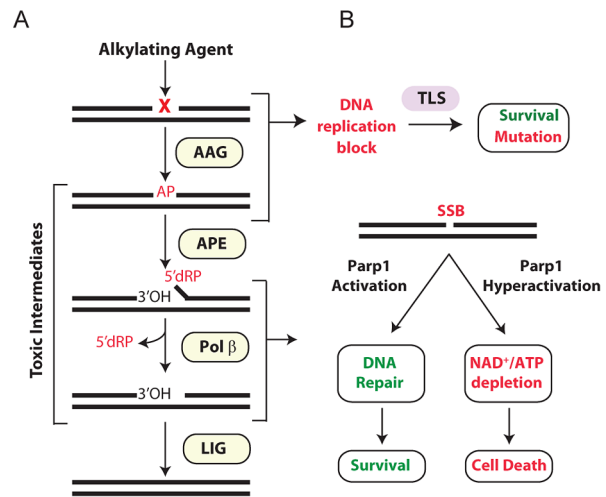


Figure 1. Cellular processing and repair of DNA base lesions in DNA. (A) DNA base lesions induced by S_N1 or S_N2 alkylating agent are recognized and excised by the DNA glycosylase, Aag, to generate an AP site. The base excision repair (BER) pathway continues when an AP endonuclease cleaves the DNA backbone to generate 3' hydroxyl and 5' deoxyribose phosphate (5'dRP) termini. Polymerase β removes the 5'dRP species, and inserts the missing DNA bases; DNA ligase completes BER by sealing the nicked DNA. (B) Error-prone translesion (TLS) polymerases can assist in the tolerance or bypass of base lesions and AP sites. Parp1 has an important role in regulating the response to DNA damage. During times of moderate DNA damage, Parp1 activation facilitates BER. Upon high levels of DNA damage, Parp1 undergoes hyperactivation; cells consequently suffer NAD^+ /ATP depletion, triggering cell death.

doi:10.1371/journal.pgen.1003413.g001

MMS-induced cytotoxicity is avoided, presumably by preventing the accumulation of toxic intermediates, and by translesion DNA synthesis (TLS) bypassing lesions in replicating cells (Figure 1B).

The multi-functional protein, Parp1, mediates several cellular processes including stress responses, transcriptional regulation, and DNA SSB repair and BER [30–32]. Parp1's role as a molecular sensor of SSBs is well established; upon binding DNA breaks, Parp1 adds poly(ADP-ribose) (PAR) polymers to numerous nuclear proteins including itself, DNA polymerases, DNA ligases, transcription factors, and histones [31,33]. Parp1 automodification facilitates BER by recruiting the scaffold protein XRCC1 that in turn facilitates the formation of a BER repair complex comprising APE1, DNA Pol β , and DNA ligase III [34–36]. Further, PARylation of histones, Parp1, and chromatin remodeling enzymes relaxes chromatin allowing DNA repair proteins access to damaged DNA [37–39]. Importantly, Parp1 is also a cell death mediator [12]; upon excessive levels of DNA damage, Parp1 hyperactivation vastly increases NAD^+ consumption resulting in depletion of both NAD^+ and ATP, such that cells succumb to bioenergetic failure (Figure 1B). Independent of NAD^+ /ATP depletion, the PAR polymer can also stimulate cell death by facilitating translocation of apoptosis inducing factor (AIF) from mitochondria to the nucleus, resulting in chromatin condensation, caspase-independent DNA degradation, and ultimately cell death [12,40,41]. While the various roles of Parp1 in programmed necrosis are still being elucidated, it is quite clear that Parp1 is a central player.

Imbalanced BER can arise either by increased DNA glycosylase activity, or by a decrease in any downstream BER step (reviewed in [6]). For example, decreased Pol β activity, as observed in the *Polβ*^{1265C/1265C} knock-in mice, results in an accumulation of BER

intermediates, causing severe physiological consequences [42]. Interestingly, recent studies generated imbalanced BER by both increasing Aag activity and eliminating Pol β activity; such cells displayed enhanced alkylation sensitivity [43,44]. Although BER imbalance increases alkylation sensitivity in cultured cells, the effects of BER imbalance on *in vivo* alkylation sensitivity have not yet been extensively studied. Using transgenic mice exhibiting modestly increased Aag activity, we investigated the effects of imbalanced BER in many tissues. We show that *AagTg* mice exhibit dramatic alkylation sensitivity, at both the tissue and the whole-body level, consistent with imbalanced BER leading to the accumulation of toxic intermediates. Moreover, we show that *Parp1* deficiency prevents alkylation-induced damage in numerous tissues, indicating that the Aag-dependent alkylation sensitivity observed *in vivo* occurs in a Parp1-dependent manner.

Results

Generation of *AagTg* mice to model BER imbalance *in vivo*

BER modulation has recently attracted attention as a way to potentiate alkylation sensitivity [6,30,44–48]. To investigate the consequences of imbalanced BER *in vivo*, we generated *Aag* transgenic (*AagTg*) mice; Table S1 displays the Aag activity levels in three transgenic founder (Fo) lines. Fo line 243 exhibits increased Aag activity in all tissues examined, with a ~2–9-fold increase compared to WT levels (Table S1 and Figure S1A). Fo line 8756 displays negligible increases in Aag activity in every tissue except the cerebellum. Finally, Aag activity in Fo line 943 tissues falls in-between, with 1.5–4-fold increases compared to WT levels. To add context to the range of Aag activities in our *AagTg* mice, we examined human AAG activity in peripheral blood mononuclear cells (PBMC) of healthy individuals. We observe >10-fold variation in AAG activity in this healthy population, as measured by excision of 1',N⁶ ethenoadenine (ϵ A) bases from DNA (Figure 2); ϵ A represents one of AAG's many substrates [23,26]. This wide range of AAG activity among healthy individuals is similar to that recently reported [7].

Imbalanced BER increases whole-body sensitivity to alkylating agents

AagTg mice are viable and fertile, and an aging study revealed no apparent differences in lifespan or tumor incidence between

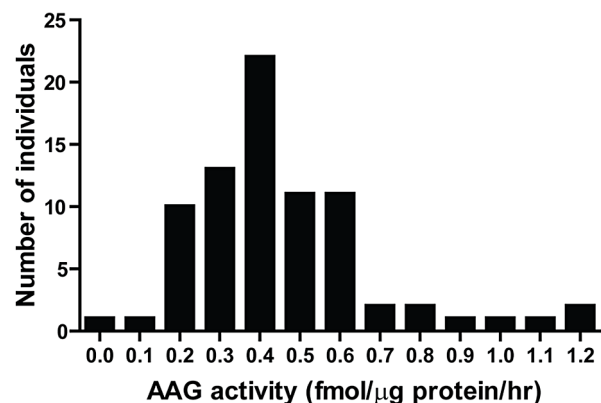


Figure 2. Human peripheral blood mononuclear cells (PBMCs) exhibit a wide range in AAG activity. An *in vitro* glycosylase assay determined AAG activity in PBMCs isolated from 80 healthy individuals. doi:10.1371/journal.pgen.1003413.g002

Table 1. Approximate MMS LD₅₀ for *Aag* transgenic mice.

Mouse Strain	MMS LD ₅₀
C57Bl/6	150 mg/kg
<i>Aag</i> ^{-/-}	150 mg/kg
<i>AagTg</i> Fo 8756*	150 mg/kg
<i>AagTg</i> Fo 943*	120 mg/kg
<i>AagTg</i> Fo 243*	80 mg/kg

*Indicates that the *Aag* transgene is expressed in an *Aag*^{-/-} background. doi:10.1371/journal.pgen.1003413.t001

WT, *Aag*^{-/-} and *AagTg* Fo line 243 (Figure S1B and data not shown). Although increased Aag activity *in vivo* does not significantly alter longevity or spontaneous tumor incidence, it does profoundly affect how mice respond to DNA damage. Similar to our previous published findings, WT and *Aag*^{-/-} mice display the same approximate LD₅₀ for MMS (150 mg/kg) (Table 1) [28]. However, *AagTg* Fo 243, with a 2–9-fold increase in Aag activity, exhibits a dramatic increase in MMS sensitivity (Table 1). Mice with intermediate Aag levels (*AagTg* Fo 943) have an intermediate LD₅₀, and *AagTg* Fo 8756, with negligible Aag activity in most tissues, exhibits the same MMS LD₅₀ as WT and *Aag*^{-/-} mice (Table 1). Therefore, increased Aag activity sensitizes animals to MMS-induced whole-body lethality.

We next determined whether Aag activity affects the approximate LD₅₀ for other genotoxic agents: N-methyl-N-nitrosourea (MNU), azoxymethane (AOM), mitomycin C (MMC), and chloroacetaldehyde (CAA). Table 2 illustrates that while the *AagTg* Fo 243 mice show dramatically increased whole-body sensitivity to three different methylating agents (MMS, MNU and AOM), they were not sensitized to non-methylating genotoxic agents (MMC and CAA). Thus, Aag activity dictates sensitivity to both S_N1 (MNU and AOM) and S_N2 methylating agents (MMS), but not to the other genotoxic agents examined. Since the increased Aag activity in *AagTg* Fo 243 mice falls within the range observed in PBMCs of a healthy human population, this founder line was chosen to further examine the consequences of BER imbalance, and are henceforth referred to as *AagTg* mice.

AagTg mice exhibit increased MMS cytotoxicity in numerous, but not all, tissues

Histopathological analysis was performed on tissues harvested from WT, *Aag*^{-/-}, and *AagTg* mice 24 h following MMS

Table 2. Approximate LD₅₀ of *Aag*^{-/-} and *Aag* transgenic mice to various genotoxic agents.

Mouse Strain	Approximate LD ₅₀				
	MMS	MNU	AOM	MMC	CAA
C57Bl/6	150 mg/kg	118 mg/kg	28 mg/kg	9 mg/kg	15.2 mg/kg
<i>Aag</i> ^{-/-}	150 mg/kg	118 mg/kg	28 mg/kg	9 mg/kg	15.2 mg/kg
<i>AagTg</i> Fo 243*	80 mg/kg	35 mg/kg	18 mg/kg	9 mg/kg	15.2 mg/kg

MMS, Methyl methanesulfonate; MNU, N-methyl-N-nitrosourea; AOM, Azoxymethane; MMC, Mitomycin C; CAA, Chloroacetaldehyde. *Indicates that the *Aag* transgene is expressed in an *Aag*^{-/-} background. doi:10.1371/journal.pgen.1003413.t002

treatment (150 mg/kg). Because massive cell death was observed in rapidly-proliferating tissues including the spleen, thymus, and bone marrow (BM) for all genotypes, we reduced the MMS dose to 75 mg/kg to better discern any differences in sensitivity in these tissues. Even with this reduced MMS dose, *AagTg* mice displayed evidence of whole-body toxicity whereas WT and *Aag*^{-/-} mice did not. Remarkably, as early as 24 h following MMS treatment, *AagTg* mice exhibit greater reductions in body weight than WT or *Aag*^{-/-} mice (Figure 3A), losing >10% of their BW by 24 h; the decreased body weight remains significantly greater than that for WT and *Aag*^{-/-} mice for over 3 weeks (Figure 3B). Moreover, 24 h following MMS treatment (75 mg/kg), we observe gross tissue atrophy in the thymus and spleen in *AagTg* mice; *AagTg* mice exhibit 46% and 53% decreases in thymus and spleen weight, respectively, compared to untreated tissues (Figure 3C). WT mice also exhibit a slight (26%) but significant decrease in spleen weight following MMS treatment but no evidence of thymic atrophy (compared to untreated WT mice). Strikingly, *Aag*^{-/-} mice are completely protected from the MMS-induced atrophy in both the thymus and spleen (Figure 3C). Further, *ex vivo* clonogenic survival assays illustrate that *AagTg* bone marrow (BM) cells display dramatically increased MMS sensitivity, compared to WT and *Aag*^{-/-} mice; as previously published, *Aag*^{-/-} BM cells are less sensitive than WT BM cells to MMS (Figure 3D) [28]. However, not all tissues that exhibit increased Aag activity reveal evidence of gross tissue atrophy. Figure S2 illustrates that tissue weights of the heart, kidney, brain, gonadal fat pad, skeletal muscle and liver remain unchanged following MMS treatment (75 mg/kg). Finally, Figure S3 illustrates that *AagTg* mice exhibit severe cell death within the pancreatic β -islets following MMS treatment (150 mg/kg), which is not observed in WT or *Aag*^{-/-} mice. The β -cells exhibit nuclear fragmentation and pyknosis, a state of increased chromatin condensation. Taken together, these results reveal that the ~2–9 fold increase in Aag activity in the thymus, spleen, BM, and pancreas relative to WT (Table S1) renders these tissues dramatically more sensitive to the toxic effects of MMS. Further, we observe increased MMS toxicity in only a subset of tissues expressing the Aag transgene, underscoring the importance of cellular context in determining MMS sensitivity in *AagTg* mice.

Unexpectedly, 24 h following a high MMS dose (150 mg/kg), we observe cell death in the cerebellar granule cells, the cell type which comprises 99% of the granular layer of the cerebellum. Following MMS treatment, there is a striking change in cerebellar morphology in *AagTg* mice. We observe severe cerebellar lesions containing numerous pyknotic nuclei surrounded by white spaces, indicative of edema (Figure 4A). Pyknotic nuclei, but not edema, are also observed, albeit at a lower frequency, in the cerebella of treated WT mice, whereas the cerebella of treated *Aag*^{-/-} mice are indistinguishable from untreated mice (Figure 4A). The regions of edema were quantitated using image analysis software; examples of colorized lesions are shown in the lowest panel of Figure 4A. In untreated mice, no edema is observed (Figure 4B). However, 24 h following MMS (150 mg/kg), there is an obvious increase in edema in *AagTg* mice compared to either WT or *Aag*^{-/-} mice, and a trend towards an increase in WT compared to *Aag*^{-/-} mice ($p = 0.308$), suggesting that *Aag*^{-/-} mice are protected against MMS-mediated cerebellar toxicity. Here we illustrate that MMS treatment results in severe cerebellar damage that is Aag-dependent. Although cerebellar damage has been described following treatment of early postnatal mice (PND3) with the alkylating agents methylazoxymethanol and mechlorethamine, to our knowledge, it has not previously been demonstrated following treatment of adult mice [49,50].

Aag-dependent, MMS-induced cerebellar degeneration results in impaired motor function

Given the importance of the cerebellum in coordinating motor function, we investigated whether MMS-induced cerebellar lesions result in diminished motor control. Decreased mobility was observed in all genotypes following a high MMS dose (150 mg/kg) (data not shown), so we reduced the MMS dose (90 mg/kg) for gait comparisons between WT, *Aag*^{-/-}, and *AagTg* mice. The gait of all genotypes was indistinguishable under untreated conditions (Figure S4). However, three hours following MMS treatment, the gait of WT and *Aag*^{-/-} mice is unchanged whereas *AagTg* mice exhibit severe gait abnormalities including immobility, circling, and walking backwards (Figure 5A). We quantitated motor defects by performing an accelerating speed rotarod test. To ensure all genotypes were capable of performing for >30 seconds on the rotarod test, we further reduced the MMS dose (60 mg/kg). Without MMS exposure, all genotypes performed comparably (Figure 5B). However, three hours following MMS treatment, we observed a dramatic decrease in rotarod performance for *AagTg* mice compared to WT and *Aag*^{-/-} mice (Figure 5B). Although the *AagTg* mice slightly improved their performance by 4 hours, it remained significantly decreased compared to WT and *Aag*^{-/-} mice (Figure 5B). Treated WT and *Aag*^{-/-} mice performed similarly to untreated mice, indicating that MMS at this dose (60 mg/kg) caused no motor dysfunction in WT or *Aag*^{-/-} mice.

We next increased the MMS dose to one that resulted in obviously impaired motor function in WT mice (140 mg/kg), and again examined motor function using the rotarod test (Figure 5C); the *AagTg* mice could not be included in this experiment due to their extreme sensitivity at this MMS dose. Strikingly, even at this high dose, *Aag*^{-/-} mice remain completely protected against MMS-induced motor dysfunction; they not only exhibit significantly better performance than WT mice, but their performance following MMS remains the same as in untreated conditions (Figure 5C). This observation is consistent with the absence of histological cerebellar lesions in *Aag*^{-/-} mice following MMS (150 mg/kg) treatment (Figure 4A). Together, these data underscore the importance of BER coordination in neuronal homeostasis; MMS induces cerebellar degeneration that is exacerbated by imbalanced BER in *AagTg* mice. Perhaps most importantly, the elimination of BER initiation in *Aag*^{-/-} mice completely suppresses MMS-induced cerebellar toxicity.

The absence of Parp1 suppresses Aag-dependent MMS-induced toxicity in several tissues

Given the role for Parp1 in mediating alkylation toxicity, we next set out to determine whether eliminating Parp1 could modulate the MMS-induced cytotoxicity observed in WT and *AagTg* mice; to explore this possibility, we utilized *Parp1*^{-/-} mice [51]. We first investigated MMS-induced retinal degeneration (RD). As previously illustrated, MMS induces the selective degeneration of the photoreceptors in the retinal outer nuclear layer (ONL) in WT mice, whereas juxtaposed retinal layers are unaffected [29]. While *Aag*^{-/-} mice are completely protected from such RD, *AagTg* mice are hypersensitive compared to WT and *Aag*^{-/-} mice, as observed by decreased number of cells found within the ONL (Figure 6 and [29]). Strikingly, we observe that *Parp1*^{-/-} mice are also completely protected against MMS-induced RD (Figure 6). Moreover, MMS-induced RD is completely abrogated in *AagTg/Parp1*^{-/-} mice, indicating that Parp1 deficiency completely suppresses the Aag-dependent MMS-hypersensitivity in photoreceptors of *AagTg* mice (Figure 6). To confirm that Parp1 enzymatic activity is stimulated during MMS-

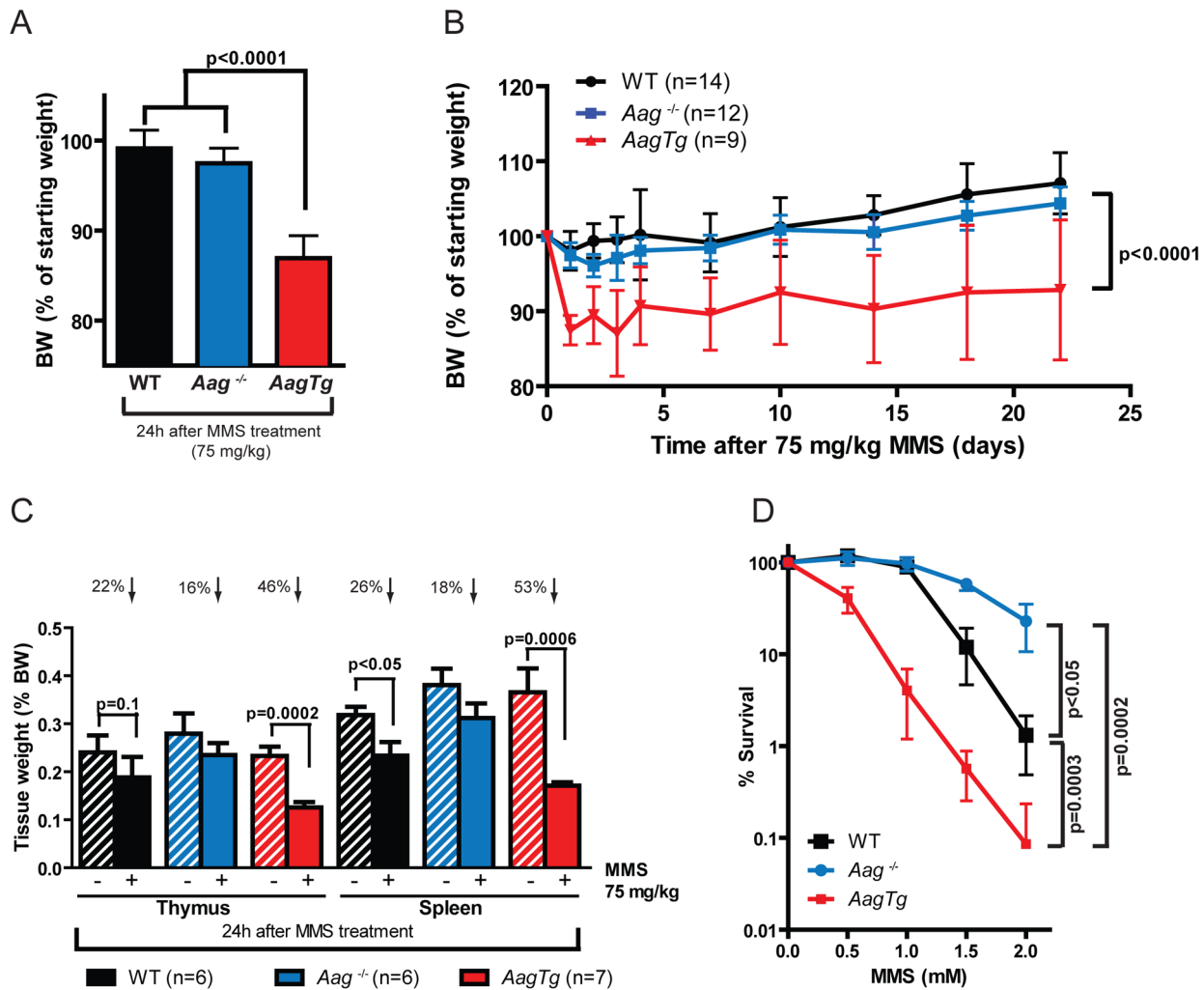


Figure 3. *AagTg* mice are more susceptible to MMS-induced toxicity. (A) Body weight (BW) of WT (n = 14), *Aag*^{-/-} (n = 12) and *AagTg* (n = 12) mice 24 h following MMS treatment (75 mg/kg). Representative data (mean ± standard deviation) from 3 independent experiments are shown. (B) BW is illustrated for WT (n = 14), *Aag*^{-/-} (n = 12) and *AagTg* (n = 9) mice following MMS treatment (75 mg/kg). Data represent mean ± standard deviation. (C) Tissue weights of spleen and thymus are illustrated for n > 6 per genotype. Striped bars represent untreated tissue weights and solid bars represent tissue weights 24 h following MMS treatment (75 mg/kg). Percent decrease in tissue weight observed following MMS treatment is shown above bars. Data represent mean ± SEM. (D) *Ex vivo* bone marrow (BM) clonogenic survival assays were performed using BM isolated from WT (n = 3), *Aag*^{-/-} (n = 3) and *AagTg* (n = 3). Data represent mean ± SEM. All the mice used in this figure are males on a pure C57BL/6 background. doi:10.1371/journal.pgen.1003413.g003

induced Aag-dependent RD, we evaluated Parp1 activation by immunodetection of the PAR polymer. Figure S5 shows that increased PAR polymer staining is observed 24 h following MMS treatment, in an Aag-dependent manner, confirming that MMS-induced RD is preceded by Parp1 activation. Similarly, we observe that *Parp1* deficiency is able to suppress the pancreatic β -cell death observed in *AagTg* mice following an acute MMS treatment (Figure S6). Together, these data indicate that the BER intermediates exert their toxicity through the hyperactivation of Parp1. Further, we find that deletion of Parp1 prevents MMS-induced toxicity and that both Aag and Parp1 are required for MMS-induced cell death.

We next investigated the requirement for Parp1 in MMS-induced cerebellar degeneration. While MMS (150 mg/kg) induces severe cerebellar lesions in *AagTg* mice (Figure 4A), Parp1 deficiency completely suppresses this Aag-dependent, alkylation-induced cerebellar toxicity (Figure 7A). Image analysis confirms that the drastic increase in the edema in MMS-treated *AagTg* mice

was completely abrogated in *AagTg/Parp1*^{-/-} mice (Figure 7B). Consistent with rescue of cerebellar lesions in *AagTg/Parp1*^{-/-} mice (Figure 7B), we illustrate using gait analysis that Parp1 deficiency prevents the motor dysfunction observed following MMS treatment in *AagTg* mice (Figure S7). Additionally, rotarod assays were performed in WT, *AagTg* and *AagTg/Parp1*^{-/-} mice to quantitate motor function. Following MMS (60 mg/kg), the motor function in WT mice remain unaffected, whereas *AagTg* mice exhibit significantly diminished performance (Figure 7C). Importantly, following MMS, *AagTg/Parp1*^{-/-} mice perform just as well as WT mice, indicating that the Aag-dependent MMS-hypersensitivity in the cerebella of *AagTg* mice is completely dependent on Parp1 (Figure 7C). Further, the Parp1 deficiency was sufficient to prevent the motor dysfunction observed at high MMS doses. As described above, at high MMS (140 mg/kg), WT mice exhibit severe motor dysfunction (Figure 5C and Figure 7D); however we find that like *Aag*^{-/-} mice, *Parp1*^{-/-} mice are protected against MMS-induced motor dysfunction and exhibit enhanced rotarod

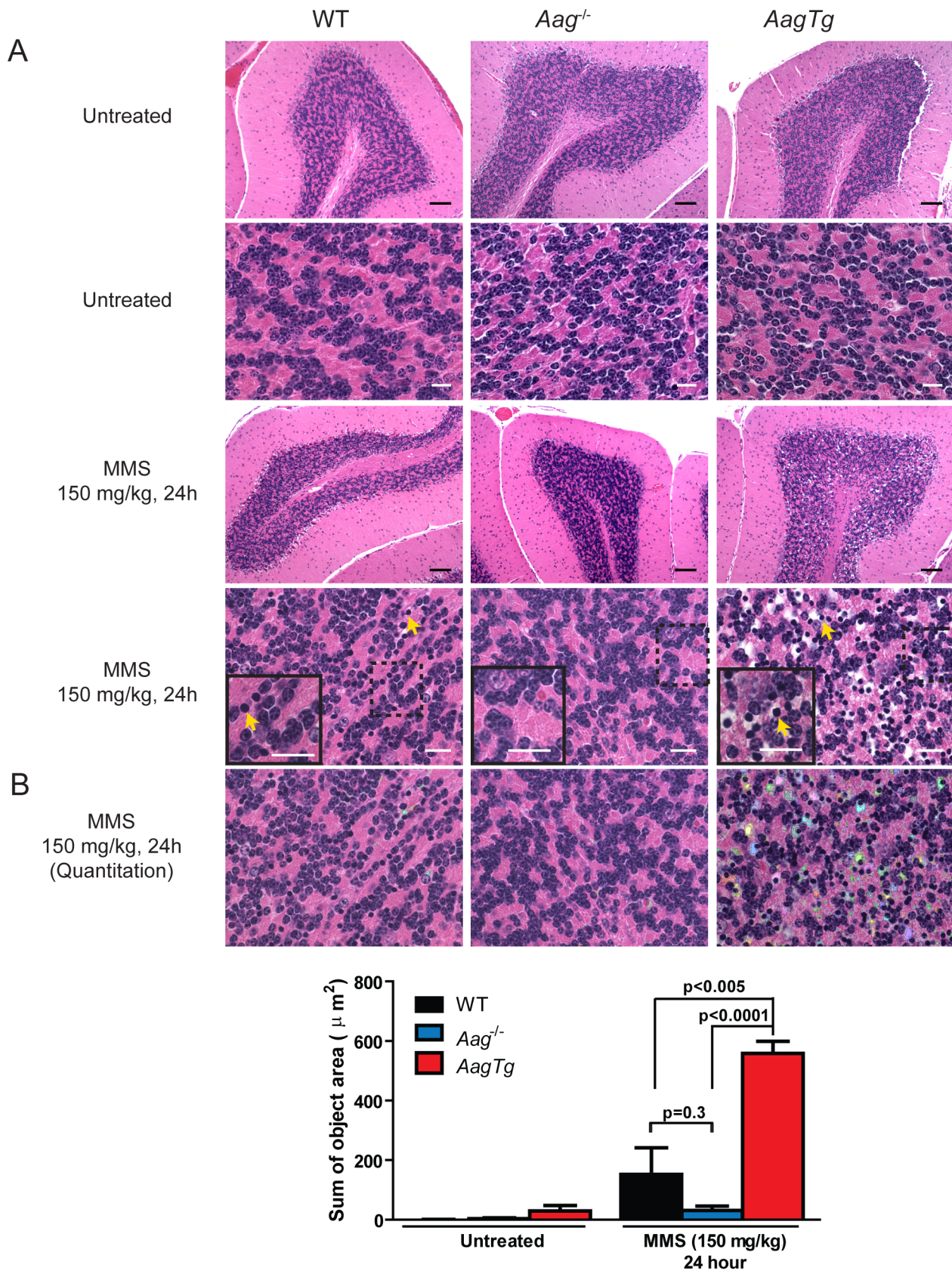


Figure 4. MMS induces severe cerebellar lesions *AagTg* mice. (A) H&E stained image of cerebellar granule cells from WT, *Aag*^{-/-} and *AagTg* mice either in untreated conditions or 24 h following MMS treatment (150 mg/kg). Representative images are shown of n>6 experiments. Yellow arrows indicate pyknotic nuclei. Scale bar is 100 μm on low magnification images (black bar) and 15 μm on high-magnification images (white bar).

Insets contain magnified images of area in dashed boxes. (B) Quantitation of cerebellar phenotype was performed on images from WT ($n=4$), $Aag^{-/-}$ ($n=3$) and $AagTg$ mice ($n=4$). Representative images with identified objects (edema) colorized for visualization. Greater than 3 images/cerebella were quantitated per mouse, and the average sum of object area per image is presented. Data represent mean \pm SEM. All the mice in this figure are on a pure C57BL/6 background.
doi:10.1371/journal.pgen.1003413.g004

performance compared to MMS-treated WT mice (Figure 7D). The mice in this experiment are on a mixed C57BL/6:129S6 background, and the slight decrease in rotarod performance observed here, compared to Figure 5, can be attributed to differences in genetic background, as previously shown [52,53]. Together, these data (Figure 6, Figure 7, and Figure S6) indicate that both Aag and Parp1 are required for the severe MMS-mediated cytotoxicity observed in retinal photoreceptors, pancreatic β -cells, and cerebellar granule cells.

Discussion

Using $AagTg$ mice, we have investigated the *in vivo* consequences of imbalanced BER. Although increased human AAG activity was recently linked to elevated lung cancer risk [7,9] and decreased survival of glioma patients [54,55], increased Aag activity in mice does not affect spontaneous tumorigenesis or overall longevity. However, dramatic *in vivo* consequences of imbalanced BER were revealed upon treating $AagTg$ mice with alkylating agents. $AagTg$ mice exhibited increased whole-animal lethality to both S_N1 and S_N2 methylating agents, but not to other genotoxic agents. Our data suggest that under basal conditions, the level of BER intermediates produced during the repair of spontaneous DNA damage is readily accommodated by the downstream BER enzymes. However, in the presence of higher levels of DNA base damage generated by alkylating agents, Aag initiates BER at a rate such that downstream BER enzymes may be unable to efficiently process the toxic BER intermediates, resulting in cell death and tissue damage, and potentially in the death of the animal (Figure 1). Therefore, it may be predicted that patients exhibiting increased AAG activity may exhibit increased sensitivity or more detrimental side-effects to alkylating chemotherapeutic agents. Indeed, AAG expression does predict temozolomide sensitivity in glioblastoma and ovarian cancer cell lines [48,56], and AAG expression inversely correlates with survival of glioma patients following treatment [54]. Together, the data presented here as well as

published findings provide justification for an epidemiological study examining alkylation sensitivity in correlation with AAG activity levels.

Imbalanced BER in $AagTg$ mice confers increased MMS sensitivity to cells in the thymus, spleen, bone marrow, retina, pancreas, and cerebellum. Further, Aag activity predicts MMS toxicity *in vivo*, such that relative sensitivities are as follows: $AagTg > WT > Aag^{-/-}$. However, Aag activity is not the sole determinant of MMS-mediated tissue cytotoxicity; numerous tissues in the $AagTg$ mice exhibit ~ 5 – 8 fold increases in Aag activity (e.g. heart, kidney, liver) but show no evidence of increased MMS sensitivity (Figure S2 and data not shown), underscoring the importance of cellular context in determining Aag-mediated alkylation sensitivity. It remains to be determined why only subsets of cell types are susceptible to Aag-mediated alkylation toxicity. In the highly-proliferative thymus, spleen, and bone marrow, unrepaired BER intermediates presumably result in replication fork collapse and DSBs, thus triggering cell death. However, pancreatic β -cells are not highly-proliferative and both the adult cerebellar granule cells and retinal photoreceptor cells are non-replicating, post-mitotic tissues [57], indicating cell death must be replication-independent. It is important to note that even within tissues exhibiting MMS sensitivity, toxicity is not uniform across all cell types in the tissue. For example, only the ONL of the retina undergoes MMS-induced degeneration whereas the juxtaposed retinal layers remain intact. Similarly, following MMS treatment, cerebellar purkinje cells remain unaffected while neighboring cerebellar granule cells are ablated. Why are some cells so sensitive, whereas others are resistant? The activity of downstream BER proteins in the sensitive cells may simply be insufficient to process accumulating BER intermediates; this and other possibilities are currently under investigation. Together, our data emphasize the concept that BER imbalance and the resulting intermediates can profoundly affect cellular and tissue homeostasis, and reveal that in certain contexts, the absence of DNA repair can actually be beneficial to an organism.

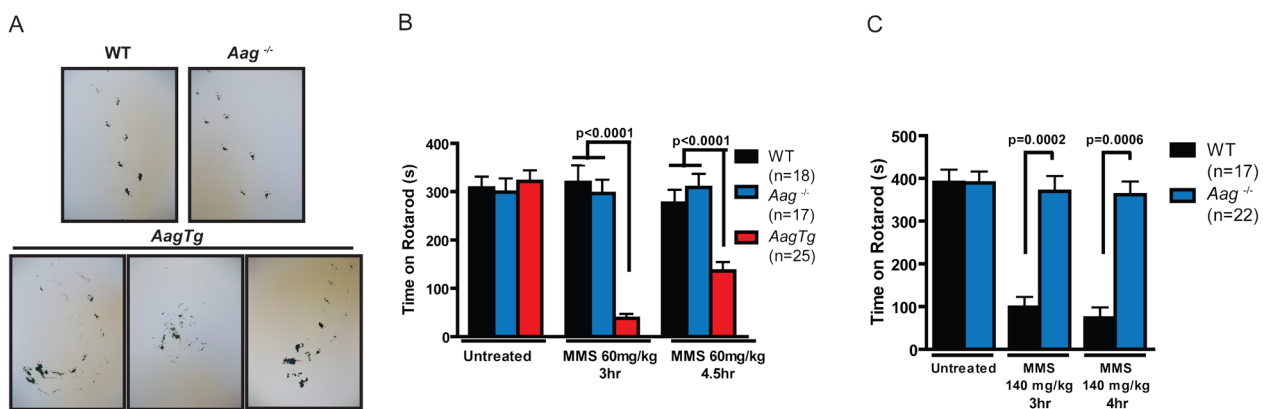


Figure 5. MMS induces an Aag-dependent decrease in motor function. (A) Representations of gait are shown for WT ($n=3$), $Aag^{-/-}$ ($n=3$) and $AagTg$ ($n=3$) mice three hours following MMS treatment (90 mg/kg). (B) Rotarod performance is shown for WT ($n=18$), $Aag^{-/-}$ ($n=17$) and $AagTg$ ($n=25$) mice under untreated conditions and following MMS treatment (60 mg/kg). Data represent mean \pm SEM. (C) Performance for the rotarod challenge is shown for WT ($n=17$) and $Aag^{-/-}$ ($n=22$), 3 and 4 h following MMS treatment (140 mg/kg). Data represent mean \pm SEM. All the mice in this figure are on a pure C57BL/6 background.
doi:10.1371/journal.pgen.1003413.g005

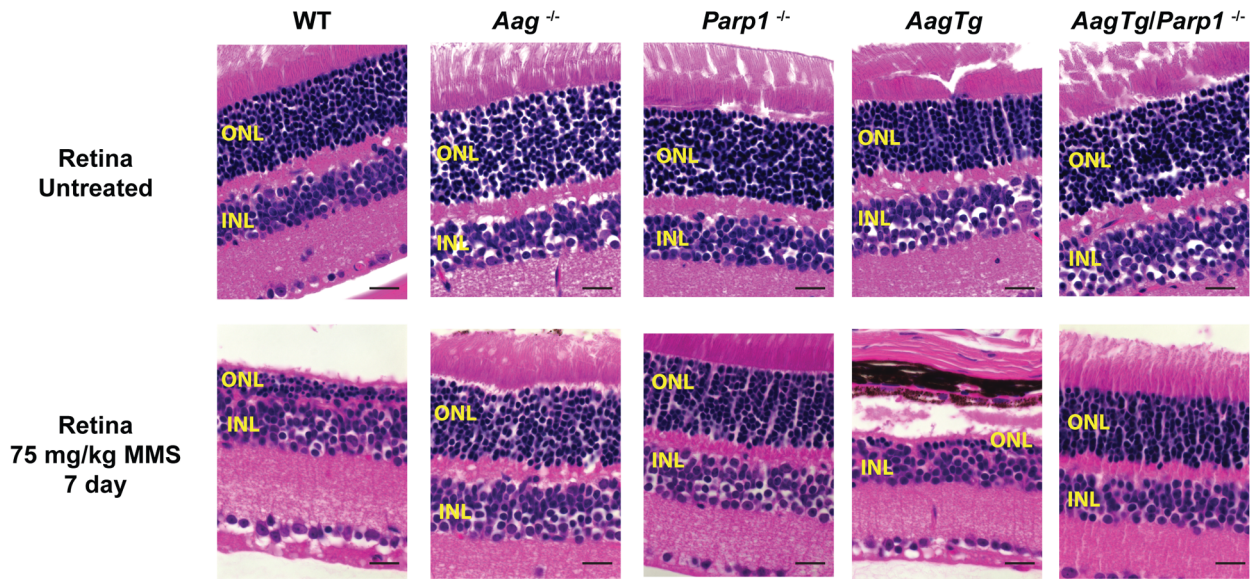


Figure 6. Parp1 deficiency protects against Aag-dependent, MMS-induced toxicity in retina photoreceptors. H&E stained retinal sections for WT, *Aag*^{-/-}, *Parp1*^{-/-}, *AagTg*, and *AagTg/Parp1*^{-/-} under untreated conditions or 7 d following MMS treatment (75 mg/kg). Scale bar is 15 μ m. Representative images for n=5 mice/genotype are shown. All the mice used in this figure are mixed C57BL/6:129S background. ONL, Outer nuclear layer; INL, inner nuclear layer.
doi:10.1371/journal.pgen.1003413.g006

Although it has been known for 30 years that Parp inhibition potentiates alkylation-induced toxicity [58], the recent discovery of synthetic lethality in BRCA1/2 homologous recombination-deficient tumors upon Parp inhibition has renewed intense interest in using PARP inhibitors for cancer chemotherapy [59,60]. However, in stark contrast to this well-documented potentiation of alkylation toxicity by Parp inhibitors [30,61], we observe complete suppression of alkylation toxicity by genetic deletion of Parp1. This is likely due to multiple inherent differences between Parp1 deficiency and Parp inhibition [62]. The main difference is the proposed trapping of Parp1 on DNA substrates by Parp inhibitors, which thereby prevents BER and interferes with replication [63,64]. Although this ‘DNA trapping’ phenomenon has been demonstrated for many Parp inhibitors, it may not be the case for all Parp inhibitors [64–67]. In fact, uncovering the relationship between the inhibition of the catalytic activity of Parp, the potency of DNA trapping, and overall toxicity by Parp inhibitors has recently garnered interest [66]. Another difference between Parp1 deficiency and Parp inhibition resides in the fact that Parp inhibitors are not specific for the inhibition of Parp1, but can potentially inhibit the catalytic activity of 17 other members of the Parp superfamily [68]. Regardless of the differences between Parp1 deletion and Parp inhibition, suppression of alkylation toxicity upon treatment of cultured cells with Parp inhibitors is not unprecedented [43,69–71].

Although Parp1 deficiency mechanistically differs from Parp inhibition, it was surprising to observe that Parp1 deficiency was capable of completely suppressing MMS hypersensitivity in numerous tissues under conditions of imbalanced BER (*AagTg* mice). This *in vivo* data reveals that Parp1 acts downstream of Aag to govern alkylation sensitivity, presumably through Parp1’s alternate function in mediating programmed necrosis (Figure 1B) [12,71]. Interestingly, interrupting Parp1’s function has been shown to be protective in several other models of neuronal damage including ischemia/reperfusion and glutamate excitotoxicity [72–74], and retinal degeneration induced by ischemia/reperfusion or

by treatment with PDE6 inhibitor, which mimics the *rd1* mutation [75,76]. Whether Aag also plays a role upstream from Parp1 in these modes of tissue damage remains to be determined.

Using genetic experiments, we show here that modestly increased Aag activity results in dramatic increases in tissue and whole-animal sensitivity to alkylating agents. Given that human AAG activity varies greatly among healthy individuals (Figure 2), and also that BER protein levels are known to be altered in numerous human cancers [77–79], the resulting imbalanced BER may have dramatic consequences in patients undergoing chemotherapy involving alkylating agents [6]. Moreover, PARP1 expression and activity varies greatly in human tumors [80], and SNPs in *PARP1* have been associated with numerous cancers [81–83]. We illustrate that Parp1 deficiency protects against alkylation sensitivity at both the tissue and whole-animal level. Therefore, decreased PARP1 activity may result in a decreased response during a chemotherapeutic regimen. Indeed, leukemic patients expressing decreased PARP1 levels exhibit resistance to standard chemotherapy therapy [84,85]. Taken together, our findings illustrate that monitoring for both BER imbalance and PARP1 expression is warranted prior to selecting a chemotherapeutic regimen that includes alkylating agents.

Materials and Methods

Ethics statement

The MIT Committee on the Use of Humans as Experimental Subjects reviewed and approved the research involving human subjects. Written informed consent was obtained from all participants. All animal procedures were approved by the MIT Committee on Animal Care.

Animals

Aag^{-/-} and *Aag* transgenic (*AagTg*) mice were described previously [21,29]. *Parp1*^{-/-} mice (Jackson Laboratories) were described previously [51]. Mice were fed a standard diet *ad libitum*,

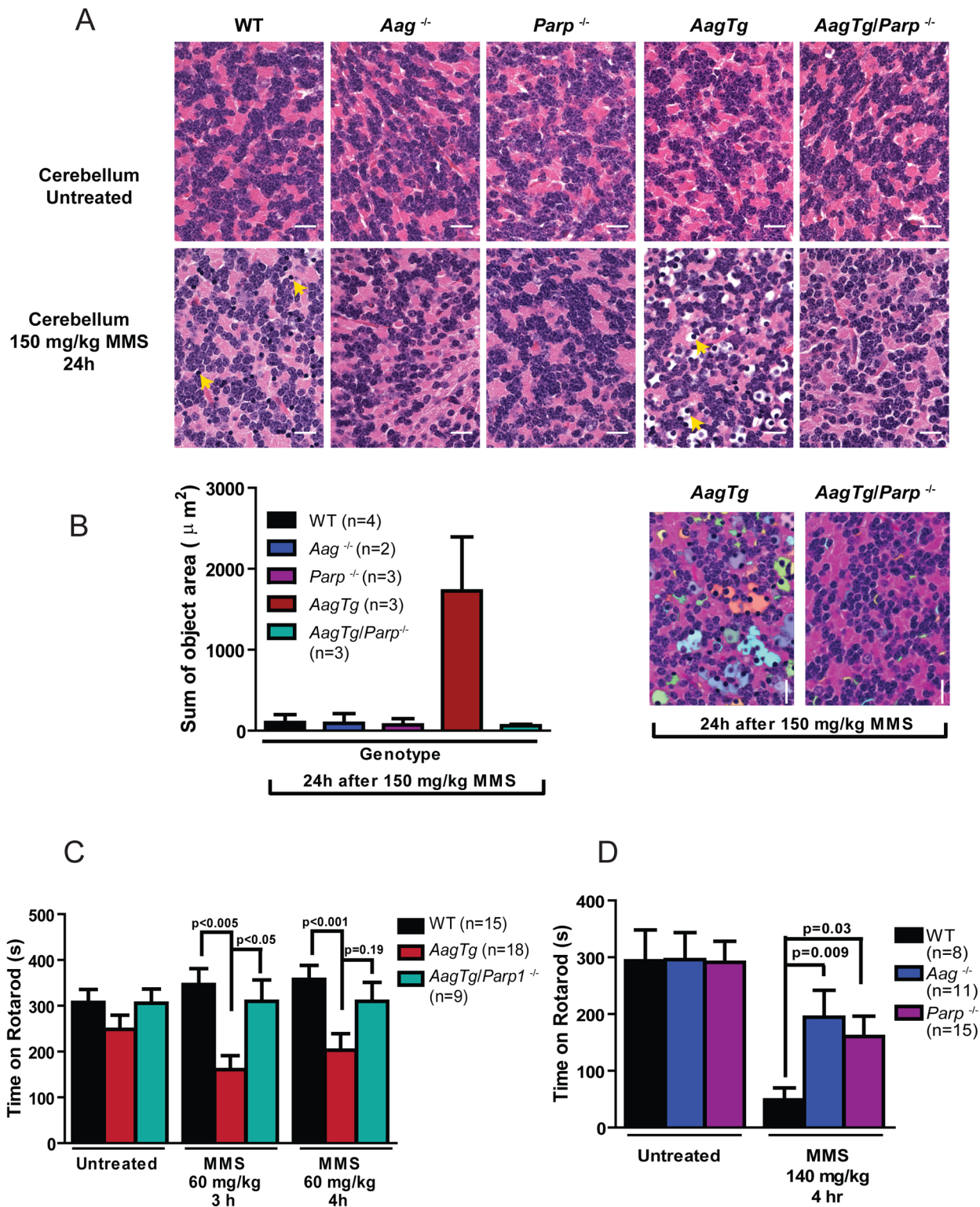


Figure 7. Parp1 deficiency protects against Aag-dependent, MMS-induced motor dysfunction. (A) H&E stained cerebellar sections are shown from WT, *Aag*^{-/-}, *Parp1*^{-/-}, *AagTg*, and *AagTg/Parp1*^{-/-} under untreated conditions or 24 h following MMS treatment (150 mg/kg). Scale bar is 15 μm. Representative images for n=5 mice/genotype are shown. (B) Quantitation of cerebellar phenotype is shown. Three or more images/cerebella were quantitated per mouse, and 3 mice per genotype analyzed for quantitation; the average sum of object area (edema) per image is presented. (C) Performance during the rotarod challenge in WT (n=15), *AagTg* (n=18), and *AagTg/Parp1*^{-/-} (n=9) is illustrated under untreated conditions and following MMS treatment (60 mg/kg). (D) Performance for the rotarod challenge is shown for WT (n=8), *Aag*^{-/-} (n=11), and *Parp1*^{-/-} (n=15) mice four hours following MMS treatment (140 mg/kg). All the mice used in this figure are mixed C57BL/6:129SvEv background. All data represent mean ± SEM.
doi:10.1371/journal.pgen.1003413.g007

housed in an AAALAC-accredited facility, and euthanized by CO₂ asphyxiation. Additional details about the mice utilized are included in the Methods S1.

Reagents

Methyl methanesulfonate (MMS), chloroacetaldehyde (CAA), N-methyl-N-nitrosourea (MNU), and Mitomycin C (MMC) were obtained from Sigma (St. Louis, MO). Azoxymethane (AOM) was obtained from the Midwest Research Institute, NCI Chemical Repository.

Treatments

Approximate LD₅₀ (whole-animal sensitivity to genotoxic agents) was determined as in Deichmann and LeBlanc [86]. Acute MMS treatments were performed by i.p. injecting mice with varying doses of MMS (60–150 mg/kg).

Tissue processing and histopathology

Tissues were processed at the David H. Koch Institute for Integrative Cancer Research, Histology Core Facility; they were paraffin-embedded, sectioned at 5 μm, and stained with hematoxylin and eosin (H&E). All H&E stained slides were blindly analyzed by a pathologist (R.T.B) for the cause of death as well as for the identification of any tumors/lesions.

Image quantitation

Volocity (Perkin Elmer) image analysis software was used to quantitate edema, as observed by white spaces in cerebellar histological sections. Thresholding was performed using the Red/Green/Blue quantitation tool and objects smaller than 5 microns were excluded. The sum of all object areas/image was calculated and greater than 3 representative images were analyzed for each of 3 animals.

Ex vivo bone marrow clonogenic assays

Bone marrow cells were harvested from the femurs of 6–12 weeks old WT, *Aag*^{-/-} and *AagTg* mice. Cells were treated with varying dose of MMS, washed, resuspended in complete media mixed with methylcellulose (Stem Cell Technologies), plated in duplicate and the percent survival calculated as in [28]. Experiments were performed in triplicate.

Evaluation of Aag activity in mouse tissues

Cell extracts were made from tissues harvested from WT, *AagTg*, and *Aag*^{-/-} mice. Tissues were sonicated in Aag glycosylase assay buffer (20 mM Tris-Cl pH 7.6, 100 mM KCl, 5 mM EDTA, 1 mM EGTA and 5 mM β-mercaptoethanol) with protease inhibitors. Protein concentration was measured using micro BCA Kit (Pierce). Glycosylase assays were performed as previously published [21]. A [³²P]γ-labeled double-stranded 25mer oligonucleotide containing a single centrally located hypoxanthine residue [5'-GCAATCTAGCTTTTT(Hx)C-GATGTATGC-3'] was incubated with an amount of extract determined to be in the linear range for activity at 37°C for 1 h. The resulting AP sites were cleaved by incubation with 0.1 N NaOH at 70 °C for 20 min. A phosphorimager was used to visualize and quantitate Aag DNA glycosylase activity.

Evaluation of AAG activity in PBMC

Peripheral blood samples were obtained from healthy individual at the MIT Catalyst Clinical Research Center, and PBMC were isolated using standard Ficoll-Paque (Sigma) density gradient centrifugations. The glycosylase assay was performed as above

with the following exceptions; the [³²P]γ-labeled lesion-containing oligonucleotide used was 5'-GCAATCTAGCCA(εA)GTC-GATGTATGC-3', and the glycosylase reaction was incubated for 37°C for 2 h.

Evaluation of motor function

To capture gait abnormalities, the mouse hind paws were dipped into non-toxic paint; mice were placed in a closed container on a sheet of white paper and allowed to walk freely. The Ugo Basile 7650 Accelerating Rotarod was used to evaluate fore-limb and hind-limb motor coordination. The rotarod testing protocol was two weeks long; the first week examined motor function under untreated conditions and the second week following MMS-treatment. An accelerating speed rotarod protocol was used, which linearly accelerates the rotating rod from 4 to 40 RPM in 10 minutes. During each week, day 1 to 4 consisted of training the mice for two 5-minute runs to familiarize the mice with the apparatus. On day 5, the mice underwent two tests, with an hour rest between the tests; the time spent on the rotarod is recorded as a measurement of performance. The 2nd week follows the same schedule, 4 days training and test on the fifth day. However, on the 5th day of the second week, the mice were treated with either 60 or 140 mg/kg MMS by i.p. injection and the test performed 3 and 4–4.5 hours post-treatment.

Immunofluorescence

5 μm unstained sections were deparaffinized and rehydrated in a graded ethanol series, incubated in citrate buffer and thermally processed for epitope retrieval. Sections were permeabilized three times (5 minutes) with PBS-T (1 × PBS+0.1% Triton X-100). Non-specific antibody binding sites were blocked by incubating sections with 1 × PBS-T+heat-inactivated goat serum (HIGS; 10%) for 30 minutes. Sections were then incubated with primary anti-PAR antibody (1:250; BD Pharmingen) for 2 hours at RT. After 5 washes in PBS-T, sections were incubated for 30 min with secondary antibody DyLight 488 (1:1000; Vector Labs). Nuclear counterstaining was done using TOPRO-3 (Invitrogen). All staining was performed in humidified chambers. A Zeiss Axiovert LSM 510 META confocal microscope (Germany) with a 63 × oil objective was used to image the retinal sections. Images were viewed and analyzed using LSM Image Browser.

Statistics

Statistical analyses were performed using GraphPad Prism software. Data are presented as mean ± SEM or mean ± SD (as stated in figure legends). Statistical significance was determined using unpaired t-test or two-way ANOVA. Kaplan-Meier survival curves were generated and survival differences determined using the Log-Rank test. A p-value is considered significant if less than 0.05.

Supporting Information

Figure S1 Evaluation of *AagTg* mice. (A) Aag activity is illustrated for a panel of tissues in WT, *Aag*^{-/-} and *AagTg* mice. *In vitro* glycosylase assays were performed on tissues isolated from n = 3 animals. (B) Kaplan Meier Survival curves are shown for an aging cohort of WT (n = 19), *Aag*^{-/-} (n = 27) and *AagTg* (n = 26) mice. (TIF)

Figure S2 Aag transgene expression does not result in MMS atrophy in all tissues. Tissue weights of the heart, left kidney, brain, left gonadal fat pad, and left gastrocnemius/soleus skeletal muscles

were taken in untreated and 24 h post MMS treatment (75 mg/kg). The mice utilized in this experiment were age-matched males on a pure C57Bl/6 background.

(TIF)

Figure S3 MMS induces pancreatic β -cell death *AagTg* mice. H&E stained slides of pancreatic β -islets (outlined in yellow) from WT, *Aag*^{-/-} and *AagTg* mice either in untreated conditions or 24 h following MMS treatment (150 mg/kg). Untreated sections show healthy pancreatic histology. Following MMS treatment, only *AagTg* exhibit evidence of toxicity within the β -cells, as illustrated by pyknotic and fragmented nuclei (shown by yellow arrows). Very few intact nuclei are observed in the pancreatic β -islet of the MMS-treated *AagTg* mice (green arrows). Representative images are shown of n>3 experiments. Scale bar is 12 μ m.

(TIF)

Figure S4 Untreated mice exhibit similar gait. Representations of gait are shown for WT (n = 3), *Aag*^{-/-} (n = 3), and *AagTg* (n = 3) mice prior to MMS treatment.

(TIF)

Figure S5 Aag-dependent Parp1 activation is observed in the retinal outer nuclear layer (ONL) following MMS treatment. Immunofluorescence staining with α -PAR antibody and TOPRO nuclear counterstain was performed on retinal sections from WT, *Aag*^{-/-} and *AagTg* mice 24 h following MMS (75 mg/kg) treatment. ONL, outer nuclear layer; INL, inner nuclear layer.

(TIF)

Figure S6 Parp1 deficiency protects against alkylation-induced pancreatic β -cell death *AagTg* mice. H&E stained slides of pancreatic β -islets from WT, *Aag*^{-/-}, *Parp1*^{-/-}, *AagTg*, and *AagTg/Parp1*^{-/-} mice either in untreated conditions or 24 h following MMS treatment (150 mg/kg). Representative images

are shown of n>2 experiments. The pancreatic β -islets are centered in image and surrounded by pancreatic acinar cells. Untreated sections show healthy pancreatic histology. Following MMS treatment, only *AagTg* exhibit evidence of pancreatic β -cell toxicity, as illustrated by pyknotic and fragmented nuclei (yellow arrow). Very few intact nuclei are observed in the pancreatic β -islet of the MMS-treated *AagTg* mice (green arrows). Magnification is 60 \times ; scale bar is 16 μ m.

(TIF)

Figure S7 Parp1 deficiency protects against alkylation-induced gait abnormalities. Representations of gait are shown for WT (n = 3), *Parp1*^{-/-} (n = 2), *AagTg* (n = 3) and *AagTg/Parp1*^{-/-} (n = 2) mice shown three hours following MMS treatment (90 mg/kg).

(TIF)

Methods S1 Supplemental Materials and Methods.

(DOCX)

Table S1 Aag activity in Aag transgenic founder lines.

(DOCX)

Acknowledgments

We thank Alicia Caron and Weijia Zhang at the David H. Koch Institute for Integrative Cancer Research Histology Core for technical help. The MIT Catalyst Clinical Research Center, especially Catherine Ricciardi, provided excellent technical assistance with our human study.

Author Contributions

Conceived and designed the experiments: JAC LBM LDS. Performed the experiments: JAC CAM-E AL LWE DS IJ PL LBM. Analyzed the data: JAC CAM-E DS RTB LBM. Contributed reagents/materials/analysis tools: DCC. Wrote the paper: JAC LDS.

References

- Hoeijmakers J (2009) DNA damage, aging, and cancer. *N Engl J Med* 361: 1475–1485.
- Hewish M, Lord CJ, Martin SA, Cunningham D, Ashworth A (2010) Mismatch repair deficient colorectal cancer in the era of personalized treatment. *Nat Rev Clin Oncol* 7: 197–208.
- Roy R, Chun J, Powell SN (2012) BRCA1 and BRCA2: important differences with common interests. *Nat Rev Cancer* 12: 372.
- McKinnon PJ (2009) DNA repair deficiency and neurological disease. *Nature reviews Neuroscience* 10: 100–112.
- Katyal S, McKinnon PJ (2008) DNA strand breaks, neurodegeneration and aging in the brain. *Mech Ageing Dev* 129: 483–491.
- Fu D, Calvo JA, Samson LD (2012) Balancing repair and tolerance of DNA damage caused by alkylating agents. *Nat Rev Cancer* 12: 104–120.
- Crosbie PA, Watson AJ, Agius R, Barber PV, Margison GP, et al. (2012) Elevated N3-methylpurine-DNA glycosylase DNA repair activity is associated with lung cancer. *Mutat Res* 732: 43–46.
- Cerda SR, Turk PW, Thor AD, Weitzman SA (1998) Altered expression of the DNA repair protein, N-methylpurine-DNA glycosylase (MPG) in breast cancer. *FEBS Lett* 431: 12–18.
- Leitner-Dagan Y, Sevilva Z, Pinchev M, Kramer R, Elinger D, et al. (2012) N-Methylpurine DNA Glycosylase and OGG1 DNA Repair Activities: Opposite Associations With Lung Cancer Risk. *J Natl Cancer Inst* 104(22): 1765–1769. doi:10.1093/jnci/djs445
- Robertson AB, Klungland A, Rognes T, Leiros I (2009) DNA repair in mammalian cells: Base excision repair: the long and short of it. *Cell Mol Life Sci* 66: 981–993.
- Boiteux S, Guillet M (2004) Abasic sites in DNA: repair and biological consequences in *Saccharomyces cerevisiae*. *DNA Repair (Amst)* 3: 1–12.
- Andrabi SA, Dawson TM, Dawson VL (2008) Mitochondrial and nuclear cross talk in cell death: parthanatos. *Ann N Y Acad Sci* 1147: 233–241.
- Schaaper RM, Kunkel TA, Loeb LA (1983) Infidelity of DNA synthesis associated with bypass of apurinic sites. *Proc Natl Acad Sci U S A* 80: 487–491.
- Pağs V, Johnson RE, Prakash L, Prakash S (2008) Mutational specificity and genetic control of replicative bypass of an abasic site in yeast. *Proc Natl Acad Sci U S A* 105: 1170–1175.
- Avkin S, Adar S, Blander G, Livneh Z (2002) Quantitative measurement of translesion replication in human cells: Evidence for bypass of abasic sites by a replicative DNA polymerase. *Proc Natl Acad Sci U S A* 99: 3764–3769.
- Goodman MF, Creighton S, Bloom LB, Petruska J, Kunkel TA (1993) Biochemical Basis of DNA Replication Fidelity. *Critical Reviews in Biochemistry and Molecular Biology* 28: 83–126.
- Strauss BS (1991) The 'A rule' of mutagen specificity: a consequence of DNA polymerase bypass of non-instructional lesions? *Bioessays* 13: 79–84.
- Sobol RW, Prasad R, Evenski A, Baker A, Yang X-P, et al. (2000) The lyase activity of the DNA repair protein [beta]-polymerase protects from DNA-damage-induced cytotoxicity. *Nature* 405: 807–810.
- Sobol RW, Kartalou M, Almeida KH, Joyce DF, Engelward BP, et al. (2003) Base excision repair intermediates induce p53-independent cytotoxic and genotoxic responses. *J Biol Chem* 278: 39951–39959.
- Saparbaev M, Laval J (1994) Excision of hypoxanthine from DNA containing dIMP residues by the *Escherichia coli*, yeast, rat, and human alkylpurine DNA glycosylases. *Proc Natl Acad Sci U S A* 91: 5873–5877.
- Engelward BP, Weeda G, Wyatt MD, Broekhof JL, de Wit J, et al. (1997) Base excision repair deficient mice lacking the Aag alkyladenine DNA glycosylase. *Proc Natl Acad Sci U S A* 94: 13087–13092.
- Gallagher PE, Brent T.P. (1984) Further purification and characterization of human 3-methyladenine-DNA glycosylase. Evidence for broad specificity. *Biochim Biophys Acta* 782: 394–401.
- Hang B, Singer B, Margison GP, Elder RH (1997) Targeted deletion of alkylpurine-DNA-N-glycosylase in mice eliminates repair of 1,N6-ethenoadenine and hypoxanthine but not of 3,N4-ethenocytosine or 8-oxoguanine. *Proc Natl Acad Sci U S A* 94: 12869–12874.
- Miao F, Bouziane M, O'Connor TR (1998) Interaction of the recombinant human methylpurine-DNA glycosylase (MPG protein) with oligodeoxynucleotides containing either hypoxanthine or abasic sites. *Nucleic Acids Res* 26: 4034–4041.
- O'Connor TR (1993) Purification and characterization of human 3-methyladenine-DNA glycosylase. *Nucleic Acids Res* 21: 5561–5569.
- Lee CY, Delancy JC, Kartalou M, Lingaraju GM, Maor-Shoshani A, et al. (2009) Recognition and processing of a new repertoire of DNA substrates by human 3-methyladenine DNA glycosylase (AAG). *Biochemistry* 48: 1850–1861.
- Fu D, Samson LD (2012) Direct repair of 3,N(4)-ethenocytosine by the human ALKBH2 dioxygenase is blocked by the AAG/MPG glycosylase. *DNA Repair (Amst)* 11: 46–52.
- Roth RB, Samson LD (2002) 3-Methyladenine DNA glycosylase-deficient Aag null mice display unexpected bone marrow alkylation resistance. *Cancer Res* 62: 656–660.

29. Meira LB, Moroski-Erkul CA, Green SL, Calvo JA, Bronson RT, et al. (2009) Aag-initiated base excision repair drives alkylation-induced retinal degeneration in mice. *Proc Natl Acad Sci U S A* 106: 888–893.
30. Rouleau M, Patel A, Hendzel MJ, Kaufmann SH, Poirier GG (2010) PARP inhibition: PARP1 and beyond. *Nat Rev Cancer* 10: 293–301.
31. Schreiber V, Dantzer F, Ame JC, de Murcia G (2006) Poly(ADP-ribose): novel functions for an old molecule. *Nat Rev Mol Cell Biol* 7: 517–528.
32. Krishnakumar R, Gamble MJ, Frizzell KM, Berrocal JG, Kininis M, et al. (2008) Reciprocal Binding of PARP-1 and Histone H1 at Promoters Specifies Transcriptional Outcomes. *Science* 319: 819–821.
33. Kraus WL, Lis JT (2003) PARP Goes Transcription. *Cell* 113: 677–683.
34. El-Khamisy SF, Masutani M, Suzuki H, Caldecott KW (2003) A requirement for PARP1 for the assembly or stability of XRCC1 nuclear foci at sites of oxidative DNA damage. *Nucleic Acids Research* 31: 5526–5533.
35. Masson M, Niedergang C, Schreiber V, Muller S, Menissier-de Murcia J, et al. (1998) XRCC1 Is Specifically Associated with Poly(ADP-Ribose) Polymerase and Negatively Regulates Its Activity following DNA Damage. *Mol Cell Biol* 18: 3563–3571.
36. Vidal AE, Boiteux S, Hickson ID, Radicella JP (2001) XRCC1 coordinates the initial and late stages of DNA abasic site repair through protein-protein interactions. *Embo J* 20: 6530–6539.
37. Ahel D, Horčiči Z, Wiechens N, Polo SE, Garcia-Wilson E, et al. (2009) Poly(ADP-ribose)-Dependent Regulation of DNA Repair by the Chromatin Remodeling Enzyme ALC1. *Science* 325: 1240–1243.
38. Timinsky G, Till S, Hassa PO, Hothorn M, Kustatscher G, et al. (2009) A macrodomain-containing histone rearranges chromatin upon sensing PARP1 activation. *Nat Struct Mol Biol* 16: 923–929.
39. Gottschalk AJ, Timinsky G, Kong SE, Jin J, Cai Y, et al. (2009) Poly(ADP-ribose) directs recruitment and activation of an ATP-dependent chromatin remodeler. *Proc Natl Acad Sci USA* 106: 13770–13774.
40. Heeres JT, Hergenrother PJ (2007) Poly(ADP-ribose) makes a date with death. *Curr Opin Chem Biol* 11: 644–653.
41. Joza N, Pospisilik JA, Hangen E, Hanada T, Modjtahedi N, et al. (2009) AIF: not just an apoptosis-inducing factor. *Ann N Y Acad Sci* 1171: 2–11.
42. Senejani AG, Dalal S, Liu Y, Nottoli TP, McGrath JM, et al. (2012) Y265C DNA polymerase beta knockin mice survive past birth and accumulate base excision repair intermediate substrates. *Proc Natl Acad Sci U S A* 109: 6632–6637.
43. Tang J-b, Svilar D, Trivedi RN, Wang X-h, Goellner EM, et al. (2011) N-methylpurine DNA glycosylase and DNA polymerase β modulate BER inhibitor potentiation of glioma cells to temozolomide. *Neuro-Oncology* 13: 471–486.
44. Tang J-b, Goellner EM, Wang X-h, Trivedi RN, St Croix CM, et al. (2010) Bioenergetic Metabolites Regulate Base Excision Repair-Dependent Cell Death in Response to DNA Damage. *Molecular Cancer Research* 8: 67–79.
45. Liu L, Gerson SL (2004) Therapeutic impact of methoxyamine: blocking repair of abasic sites in the base excision repair pathway. *Curr Opin Investig Drugs* 5: 623–627.
46. Wilson D, Simeonov A (2010) Small molecule inhibitors of DNA repair nuclease activities of APE1. *Cellular and Molecular Life Sciences* 67: 3621–3631.
47. Jelezcova E, Trivedi RN, Wang X-h, Tang J-b, Brown AR, et al. (2010) Parp1 activation in mouse embryonic fibroblasts promotes Pol [beta]-dependent cellular hypersensitivity to alkylation damage. *Mutation Research/Fundamental and Molecular Mechanisms of Mutagenesis* 686: 57–67.
48. Trivedi RN, Wang X-h, Jelezcova E, Goellner EM, Tang J-b, et al. (2008) Human Methyl Purine DNA Glycosylase and DNA Polymerase β Expression Collectively Predict Sensitivity to Temozolomide. *Molecular Pharmacology* 74: 505–516.
49. Kisby GE, Lesselroth H, Olivas A, Samson L, Gold B, et al. (2004) Role of nucleotide- and base-excision repair in genotoxin-induced neuronal cell death. *DNA Repair (Amst)* 3: 617–627.
50. Kisby GE, Olivas A, Park T, Churchwell M, Doerge D, et al. (2009) DNA repair modulates the vulnerability of the developing brain to alkylating agents. *DNA Repair (Amst)* 8: 400–412.
51. Wang ZQ, Auer B, Stügel L, Berghammer H, Haidacher D, et al. (1995) Mice lacking ADPRT and poly(ADP-ribose)ylation develop normally but are susceptible to skin disease. *Genes & Development* 9: 509–520.
52. Tarantino LM, Gould TJ, Druhan JP, Bucan M (2000) Behavior and mutagenesis screens: the importance of baseline analysis of inbred strains. *Mammalian Genome* 11: 555–564.
53. Brooks SP, Pask T, Jones L, Dunnett SB (2004) Behavioural profiles of inbred mouse strains used as transgenic backgrounds. I: motor tests. *Genes Brain Behav* 3: 206–215.
54. Liu C, Tu Y, Yuan J, Mao X, He S, et al. (2012) Aberrant Expression of N-Methylpurine-DNA Glycosylase Influences Patient Survival in Malignant Gliomas. *J Biomed Biotechnol* 2012: 760679. doi: 10.1155/2012/760679
55. Agnihotri S, Gajadhar AS, Ternamian C, Gorlia T, Diefes KL, et al. (2012) Alkylpurine-DNA-N-glycosylase confers resistance to temozolomide in xenograft models of glioblastoma multiforme and is associated with poor survival in patients. *The Journal of Clinical Investigation* 122: 253–266.
56. Fishel ML, He Y, Smith ML, Kelley MR (2007) Manipulation of base excision repair to sensitize ovarian cancer cells to alkylating agent temozolomide. *Clin Cancer Res* 13: 260–267.
57. Gould E (2007) How widespread is adult neurogenesis in mammals? *Nat Rev Neurosci* 8: 481–488.
58. Durkacz B, Omidiji O, Gray D, Shall S (1980) (ADP-ribose)_n participates in DNA excision repair. *Nature* 283: 593–593.
59. Bryant HE, Schultz N, Thomas HD, Parker KM, Flower D, et al. (2005) Specific killing of BRCA2-deficient tumours with inhibitors of poly(ADP-ribose) polymerase. *Nature* 434: 913–917.
60. Farmer H, McCabe N, Lord CJ, Tutt ANJ, Johnson DA, et al. (2005) Targeting the DNA repair defect in BRCA mutant cells as a therapeutic strategy. *Nature* 434: 917–921.
61. Méglin-Chanet F, Bollet M, Hall J (2010) Targeting poly(ADP-ribose) polymerase activity for cancer therapy. *Cellular and Molecular Life Sciences* 67: 3649–3662.
62. Haince J-F, Rouleau M, Hendzel MJ, Masson J-Y, Poirier GG (2005) Targeting poly(ADP-ribose)ylation: a promising approach in cancer therapy. *Trends in Molecular Medicine* 11: 456–463.
63. Strom CE, Johansson F, Uhlen M, Szegartyo CA, Erixon K, et al. (2011) Poly(ADP-ribose) polymerase (PARP) is not involved in base excision repair but PARP inhibition traps a single-strand intermediate. *Nucleic Acids Res* 39: 3166–3175.
64. Kedar PS, Stefanick DF, Horton JK, Wilson SH (2012) Increased PARP-1 Association with DNA in Alkylation Damaged, PARP-Inhibited Mouse Fibroblasts. *Molecular Cancer Research* 10: 360–368.
65. Ma W, Halweg CJ, Menendez D, Resnick MA (2012) Differential effects of poly(ADP-ribose) polymerase inhibition on DNA break repair in human cells are revealed with Epstein-Barr virus. *Proceedings of the National Academy of Sciences* 109: 6590–6595.
66. Murai J, Huang S-yN, Das BB, Renaud A, Zhang Y, et al. (2012) Trapping of PARP1 and PARP2 by Clinical PARP Inhibitors. *Cancer Research* 72: 5588–5599.
67. Strom CE, Johansson F, Uhlen M, Al-Khalili Szegartyo CA, Erixon K, et al. (2010) Poly(ADP-ribose) polymerase (PARP) is not involved in base excision repair but PARP inhibition traps a single-strand intermediate. *Nucleic Acids Res* 39(8):3166–75. doi: 10.1093/nar/gkq1241
68. Hottiger MO, Hassa PO, Lüscher B, Schuler H, Koch-Nolte F (2010) Toward a unified nomenclature for mammalian ADP-ribosyltransferases. *Trends in Biochemical Sciences* 35: 208–219.
69. Zong WX, Ditsworth D, Bauer DE, Wang ZQ, Thompson CB (2004) Alkylating DNA damage stimulates a regulated form of necrotic cell death. *Genes Dev* 18: 1272–1282.
70. Xu Y, Huang S, Liu ZG, Han J (2006) Poly(ADP-ribose) polymerase-1 signaling to mitochondria in necrotic cell death requires RIP1/TRAF2-mediated JNK1 activation. *J Biol Chem* 281: 8788–8795.
71. Ha HC, Snyder SH (1999) Poly(ADP-ribose) polymerase is a mediator of necrotic cell death by ATP depletion. *Proc Natl Acad Sci USA* 96: 13978–13982.
72. Eliasson M.J., Sampei K, Mandir AS, Hurn PD, et al. (1997) Poly(ADP-ribose) polymerase gene disruption renders mice resistant to cerebral ischemia. *Nat Med* 10: 1089–1095.
73. Mandir AS, Poitras MF, Berliner AR, Herring WJ, Guastella DB, et al. (2000) NMDA but not non-NMDA excitotoxicity is mediated by Poly(ADP-ribose) polymerase. *J Neurosci* 20: 8005–8011.
74. Yang Z, Zingarelli B, Szabo C (2000) Effect of genetic disruption of poly(ADP-ribose) synthetase on delayed production of inflammatory mediators and delayed necrosis during myocardial ischemia-reperfusion injury. *Shock* 13: 60–66.
75. Sahaboglu A, Tanimoto N, Kaur J, Sancho-Pelluz J, Huber G, et al. (2010) PARP1 Gene Knock-Out Increases Resistance to Retinal Degeneration without Affecting Retinal Function. *PLoS ONE* 5: e15495. doi:10.1371/journal.pone.0015495
76. Li C, Wang L, Kern TS, Zheng L (2012) Inhibition of poly(ADP-ribose) polymerase inhibits ischemia/reperfusion induced neurodegeneration in retina via suppression of endoplasmic reticulum stress. *Biochemical and Biophysical Research Communications* 423: 276–281.
77. Al-Attar A, Gossage L, Fareed KR, Shehata M, Mohammed M, et al. (2010) Human apurinic/aprimidinic endonuclease (APE1) is a prognostic factor in ovarian, gastro-oesophageal and pancreatico-biliary cancers. *Br J Cancer* 102: 704–709.
78. Sweasy JB, Lang T, DiMaio D (2006) Is Base Excision Repair a Tumor Suppressor Mechanism? *Cell Cycle* 5: 250–259.
79. Starcevic D, Dalal S, Sweasy JB (2004) Is There a Link Between DNA Polymerase Beta and Cancer? *Cell Cycle* 3: 996–999.
80. Zaremba T, Ketzner P, Cole M, Coulthard S, Plummer ER, et al. (2009) Poly(ADP-ribose) polymerase-1 polymorphisms, expression and activity in selected human tumour cell lines. *Br J Cancer* 101: 256–262.
81. Hao B, Wang H, Zhou K, Li Y, Chen X, et al. (2004) Identification of genetic variants in base excision repair pathway and their associations with risk of esophageal squamous cell carcinoma. *Cancer Res* 64: 4378–4384.
82. Lockett KL, Hall MC, Xu J, Zheng SL, Berwick M, et al. (2004) The ADPRT V762A genetic variant contributes to prostate cancer susceptibility and deficient enzyme function. *Cancer Res* 64: 6344–6348.
83. Zhang X, Miao X, Liang G, Hao B, Wang Y, et al. (2005) Polymorphisms in DNA base excision repair genes ADPRT and XRCC1 and risk of lung cancer. *Cancer Res* 65: 722–726.
84. Bacalini MG, Tavorolo S, Peragine N, Marinelli M, Santangelo S, et al. (2012) A subset of chronic lymphocytic leukemia patients display reduced levels of PARP1

- expression coupled with a defective irradiation-induced apoptosis. *Experimental Hematology* 40: 197–206.
85. Holleman A, Boer MLd, Kazemier KM, Beverloo HB, von Bergh ARM, et al. (2005) Decreased PARP and procaspase-2 protein levels are associated with cellular drug resistance in childhood acute lymphoblastic leukemia. *Blood* 106: 1817–1823.
86. Deichmann WB, LeBlanc T.J. (1943) Determination of the approximate lethal dose with about six animals. *Journal of Industrial Hygiene and Toxicology* 25: 415–417.